



ELSEVIER

Contents lists available at ScienceDirect

Acta Biomaterialia

journal homepage: [www.elsevier.com/locate/actbio](http://www.elsevier.com/locate/actbio)

Full length article

## Surface characterisation reveals substrate suitability for cyanobacterial phototaxis

Lourdes Albina Nirupa Julius<sup>a</sup>, Lukas Matter<sup>a</sup>, Nils Schuergers<sup>b</sup>, Johannes Lützenkirchen<sup>c</sup>, Vanessa Trouillet<sup>d</sup>, Teba Gil-Díaz<sup>c,e</sup>, Emil R. Mamleyev<sup>a</sup>, Annegret Wilde<sup>b</sup>, Vlad Badilita<sup>a,\*</sup>, Jan G. Korvink<sup>a,\*</sup>

<sup>a</sup> Institute of Microstructure Technology, Karlsruhe Institute of Technology, Hermann-von-Helmholtz-Platz 1, Eggenstein-Leopoldshafen 76344, Germany

<sup>b</sup> Institute of Biology III, University of Freiburg, Schänzlestrasse 1, Freiburg 79104, Germany

<sup>c</sup> Institute for Nuclear Waste Disposal, Karlsruhe Institute of Technology, Hermann-von-Helmholtz-Platz 1, Eggenstein-Leopoldshafen 76344, Germany

<sup>d</sup> Institute for Applied Materials and Karlsruhe Nano Micro Facility (KNMFi), Karlsruhe Institute of Technology, Hermann-von-Helmholtz-Platz 1, Eggenstein-Leopoldshafen 76344, Germany

<sup>e</sup> Institute for Geosciences, Friedrich Schiller University Jena, Burgweg 11, Jena 07749, Germany

### ARTICLE INFO

#### Article history:

Received 18 May 2022

Revised 24 September 2022

Accepted 17 October 2022

Available online xxx

#### MSC:

0000

1111

#### Keywords:

Cyanobacteria

Type IV motility

MEMS

Force-distance curves

Surface characterisation

### ABSTRACT

Cyanobacteria respond to light stimulation, activating localised assembly of type IV pili for motility. The resulting phototactic response is highly dependent on the nature of the incoming light stimulus, and the final motility parameters depend on the surface properties. Conventionally, phototaxis studies are carried out on hydrogel surfaces, such as agarose, with surface properties that vary in time due to experimental conditions. This study considers five substrates, widely utilized in microfluidic technology, to identify the most suitable alternative for performing reliable and repeatable phototaxis assays. The surfaces are characterised via a contact angle goniometer to determine the surface energy, white light interferometry for roughness, zeta-potentials and AFM force distance curves for charge patterns, and XPS for surface composition. Cell motility assays showed 1.25 times increment on surfaces with a water contact angle of 80° compared to a reference glass surface. To prove that motility can be enhanced, polydimethylsiloxane (PDMS) surfaces were plasma treated to alter their surface wettability. The motility on the plasma-treated PDMS showed similar performance as for glass surfaces. In contrast, untreated PDMS surfaces displayed close to zero motility. We also describe the force interactions of cells with the test surfaces using DLVO (Derjaguin-Landau-Verwey-Overbeek) and XDLVO (extended DLVO) theories. The computed DLVO/XDLVO force-distance curves are compared with those obtained using atomic force microscopy. Our findings show that twitching motility on tested surfaces can be described mainly from adhesive forces and hydrophobicity/hydrophilicity surface properties.

### Statement of significance

The current article focuses on unravelling the potential Micro-Electro-Mechanical System (MEMS) compatible surfaces for studying phototactic twitching motility of cyanobacteria. This is the first exhaustive

**Abbreviations:** AFM, Atomic Force Microscopy; DLVO, Derjaguin-Landau-Verwey-Overbeek; EDTA, Ethylenediaminetetraacetic acid; IPA, Isopropyl alcohol; iSCAT, Interferometric scattering microscopy; LOC, Lab-on-a-Chip; LW, Lifshitz-Van der Waals; MEMS, Micro-Electro-Mechanical Systems; OTS, Trichloro(octadecyl)silane; PAAm, Polyacrylamide; PCR, Polymerase chain reaction; PDMS, Polydimethylsiloxane; PEGDMA, Poly(ethylene glycol) dimethacrylate; PGMEA, Propylene glycol methyl ether acetate; SAM, Self Assembled Monolayer; T4P, Type IV Pili; VdW, van der Waals; VSI, Vertical Scanning Interferometer; WCA, Water Contact Angle; XDLVO, Extended DLVO; XPS, X-ray Photoelectron Spectroscopy;  $\gamma^+$ , Electron acceptor;  $\gamma^-$ , Electron donor;  $\gamma^{LW}$ , Lifshitz-van der Waals surface energy component;  $\gamma^{AB}$ , Lewis Acid-Base surface energy component;  $\gamma^{LW-AB}$ , Total surface energy component.

\* Corresponding authors.

E-mail addresses: [vlad.badilita@kit.edu](mailto:vlad.badilita@kit.edu) (V. Badilita), [jan.korvink@kit.edu](mailto:jan.korvink@kit.edu) (J.G. Korvink).

<https://doi.org/10.1016/j.actbio.2022.10.035>

1742-7061/© 2022 The Author(s). Published by Elsevier Ltd on behalf of Acta Materialia Inc. This is an open access article under the CC BY-NC-ND license (<http://creativecommons.org/licenses/by-nc-nd/4.0/>)

Please cite this article as: L.A.N. Julius, L. Matter, N. Schuergers et al., Surface characterisation reveals substrate suitability for cyanobacterial phototaxis, Acta Biomaterialia, <https://doi.org/10.1016/j.actbio.2022.10.035>

surface characterization study coupled with phototaxis experiments, to understand the forces contributing to twitching motility. The methods shown in this paper can be further extended to study other surfaces and also to other bacteria exhibiting twitching motility.

© 2022 The Author(s). Published by Elsevier Ltd on behalf of Acta Materialia Inc.  
This is an open access article under the CC BY-NC-ND license  
(<http://creativecommons.org/licenses/by-nc-nd/4.0/>)

## 1. Introduction

Cyanobacteria are an ancient group of microorganisms, whose representatives can be found nowadays in almost all ecosystems. The defining characteristic of these prokaryotes is the use of light as an energy source. Through oxygenic photosynthesis, cyanobacteria were responsible for the oxygenation of the atmosphere, enabled the evolution of higher plants, and play an important role in the carbon cycle in aquatic habitats [1]. As a consequence, in order to ensure a highly efficient photosynthetic process, cyanobacteria have developed an efficient light harvesting system and, in many cases, the ability to position themselves at favourable locations with respect to light sources. Cyanobacteria exhibit true phototaxis, that is, direct movement towards optimal illumination or away from harmful irradiation [2]. Phototactic movement over solid surfaces by most cyanobacteria is a form of *twitching motility* that is based on dynamic protein complexes, the *type IV pili* (T4P) [3–6]. These consist of extremely high aspect ratio filaments extending from the pores in the outer membrane that interact with the substrate surface [7]. Since many mechanistic aspects governing the twitching motility have not yet been fully understood, the interaction of the cyanobacteria with chemically different surfaces is of interest and relevant for both technological applications and understanding of their environmental distribution. The aim of this work is to identify the key surface characteristics influencing cell motility of cyanobacteria, with a particular focus on technologically, commonly used surfaces. While this paper focuses on cyanobacteria, we consider that our approach and the results obtained in this work can also serve as a guideline applicable to other microorganisms, such as the commonly known twitching model organism *Pseudomonas aeruginosa*.

In the present work, we conjecture that research on organisms showing twitching/T4P motility, in particular those studies that focus on the interaction between the microorganisms and their underlying support surfaces, could benefit from numerous advances in the field of lab-on-a-chip (LOC) technologies achieved during the past several decades. In 1990 Manz et al. [8] introduced the first concept that later evolved into what is known today as LOC or miniaturized total analysis systems ( $\mu$ TAS). Taking advantage of the already existing microfabrication facilities, LOC devices have gained in complexity and functionality, offering high precision in handling minute volumes of sample and reagents, exquisite control on the experimental environment, and overall expediting the analysis time in a large number of applications. Several examples of LOC real-world applications include DNA analysis [9], immunoassays [10], protein separation [11], cell analysis [12], and PCR (Polymerase chain reaction) [13]. Directly related to the present work, synthetic ecosystems to harbour tiny biotic species became feasible with the advent of nanofabrication and microfluidics. These micro-environments can be used to image single cells over prolonged duration [14], to monitor the smallest crevices that a bacterium can penetrate through [15], to record community behaviour responses [16], electron transport in a bacterium [17,18], and by replicating the environmental conditions in a LOC device, to successfully culture species that are otherwise difficult to grow under laboratory conditions, and carry out genomic analysis [19].

LOC technologies, however, have not been so widely adopted for phototaxis studies. A notable achievement was the rapid isolation of strains with improved photosynthetic efficiencies of a model green alga, *C. reinhardtii*, using competitive phototaxis in a microfluidic screening device [20]. In another report, nanoaquaria for *Phormidium*, a filamentous cyanobacterium, were fabricated by direct femtosecond laser writing in a photostructurable glass [21]. These devices were used to determine the influence of light intensity and wavelength on the gliding behaviour of *Phormidium*. Additionally, two other papers reported on the realization of microfluidic bioreactors for cell growth, or long term monitoring of cell division in cyanobacteria [22,23]. Yu et al. have built a microfluidic cell-culture device coupled to an image analysis pipeline for robust lineage reconstruction [23]. These PDMS-based microfluidic devices were coated with 0.01% polylysine for two hours to promote attachment of the bacteria. An interesting observation with this type of device was that the cells exhibit a considerably higher motility during the dark periods of the light-dark cycles, thus suggesting that the cells have enough energy in the dark. By evaluating the drag forces in microfluidic flow chambers, the adhesion forces of type IV and type I pili of *Xylella fastidiosa* have been measured [24]. Microfluidic chambers have also been used by Cruz et al. to evaluate the effect of various  $\text{Ca}^{2+}$  concentrations on the twitching speed of *X. fastidiosa* [25].

The most commonly used substrates in cyanobacterial studies are hydrogel phototaxis plates, based mainly on agar or agarose. A typical experiment involves the macroscopic observation of wavelength-dependent movement of cyanobacteria by following the movement of finger-patterned front edges of a bacterial colony on a Petri dish over several days in an incubator [26–28]. The widespread use of hydrogels was due to their exposing soft surfaces, whilst being a suitable medium providing nutrients to the cell population over long periods of time. For certain applications, however, other types of substrates are preferred instead. For example, the pilus retraction of *P. aeruginosa* mutants was imaged by interferometric scattering microscopy (iSCAT) on quartz substrates and such a method could also be useful to study the pilus movement of cyanobacteria in the presence of light [29]. However, the application of interferometric imaging to nanometric structures becomes impossible if hydrogels are used. Additionally, hydrogel substrates hinder the imaging process due to a constant drift in the microscope focal plane, caused by rapid evaporation from the surface. Apart from the optical consequences of the experimental setup, the constant evaporation was found to modify hydrogel surface properties, directly affecting the number of motile twitching cells and their velocities [30], with further consequences for the robustness of the study. Thus, the nature of the substrate surface and its stability are of critical importance when studying twitching motility in cyanobacterial colonies. Besides the common use of hydrogels to study the motility of cyanobacteria, glass [31] and collodion coated glass [32] have been used with promising results.

For detailed studies of phototaxis mechanisms it is essential to have a high degree of spatial control over various experimental conditions and stimuli such as nutrient delivery, temperature, humidity, or light. Whereas conventional hydrogel-based platforms do not offer the required control over the cell micro-environment,

Micro-Electro-Mechanical Systems (MEMS) technologies and LOC devices hold, in principle, all the cards that enable exquisite microscale spatial control over these inputs. Moreover, the field of MEMS offers a wide range of synthetic substrates, as well as a broad palette of processes to fine-tune the properties of these substrates at different levels, either through chemical composition, surface modification, or via micro and nano structuring. These opportunities have not yet been fully explored and exploited by the cyanobacteria research community. By implementing a micro-engineering approach, it is the purpose of this paper to consider several well-known MEMS-compatible substrates, to quantify the behaviour of cyanobacteria on a range of surfaces, and to analyze them in comparison to substrates traditionally used for cyanobacterial research, thus opening the door to a more wide-spread use of MEMS substrates and devices within the research community.

The present work analyzes several substrate materials, selected based on bio-compatibility, suitability for micro-fabrication processes, and optical transparency for microscope imaging. Section 2 of the manuscript details the materials used in the experiments, the experimental setups, as well as the methods for data interpretation. More specifically, in order to understand the influence of surface parameters on bacterial motility, due to the differences in the nature of the coatings, contact angle, zeta-potential, force-distance curves via AFM, rigidity, and surface composition measurements via X-ray photoelectron spectroscopy (XPS) have been conducted. All experimental results are presented in Section 3 of the manuscript, while Section 4 presents a detailed discussion and interpretation based on the outcome of the phototaxis assays complementing these results with the Derjaguin-Landau-Verwey-Overbeek (DLVO) and the extended DLVO (XDLVO) colloidal theories.

This is the first work providing an in-depth understanding of the surface characteristics suitable for phototaxis studies targeting cyanobacteria. This critical step is essential to translate phototaxis studies from bulk volatile hydrogel set-ups to more stable, confined and controllable microfluidics and LOC platforms.

## 2. Materials and methods

The materials and methods of the substrate preparation, cell handling, the measurements and the DLVO/XDLVO formulations are explained in detail in the subsequent sections. The materials used in the study are glass, SU-8, PDMS, OTS (trichloro(octadecyl)silane) and different concentrations of collodion (nitrocellulose) - 0.2%, 0.02%, 0.0135% and 0.007% in isoamyl acetate. The PDMS was prepared with 10:1, 20:1, 40:1 and 60:1 base curing agent ratios to study the effect of rigidity on motility. Additionally, 10:1 PDMS whose contact angle was tuned to approximately 40° by oxygen plasma treatment was also used as a test substrate. The surface characterization techniques include water contact angle measurements and subsequent surface energy calculations, roughness, rigidity, electrokinetic measurements and potentiometric acid/base titrations, XPS and force distance measurements using AFM. The motility of *Synechocystis* sp. PCC 6803 which is 3 µm in diameter was studied on the different test substrates. The experimental setup of the motility studies and the post-processing steps to evaluate the motility index and the velocity of the bacteria are shown in Fig. 1. We define the motility index as the ratio between the percentage of motile bacteria on a test substrate and the percentage of motile bacteria on glass. The DLVO/XDLVO force distance curves were computed using the surface energies (extracted from the contact angle measurements) and the streaming potentials. The force curves describe the force interactions of the bacterial cell body and the surface.

### 2.1. Preparation of substrates

#### 2.1.1. Collodion

Serial dilution of collodion (collodion solution for microscopy, 2% in amyl acetate, Sigma-Aldrich) in isoamyl acetate (isoamyl acetate natural, ≥97%, Sigma Aldrich) was performed to obtain concentrations of 0.2%, 0.02%, 0.0135% and 0.007%. A volume of 100 µl of the diluted solutions was dispensed onto a microscope slide and then spin-coated for 25 s with 480 rpm using a KLM spin coater (KL-SCC-200). The microscope slide was cleaned with acetone and isopropyl alcohol (IPA) and dried with nitrogen for 2 min before the spin coating. The thickness of the coating changes from 10 nm to 30 nm with increasing collodion concentration.

#### 2.1.2. OTS

A solution containing 400 µM of OTS (trichloro(octadecyl)silane ≥90%, Sigma-Aldrich) in toluene (toluene anhydrous, 99.8%, Sigma-Aldrich) was prepared in a Petri dish in an argon environment. The glass slides were placed in the solution for 2 h in a desiccator under vacuum. After the incubation period, using fresh toluene, methanol followed by IPA in a shaker for 2 min each was used for cleaning the glass slides. Finally, samples were baked at 100 °C for 30 min.

#### 2.1.3. PDMS

PDMS surfaces were prepared using a Sylgard 184 silicone elastomer kit (Dow Inc.). Rigidity variation was achieved using polymer mixtures with different base to curing agent ratios [60:1, 40:1, 20:1, 10:1, 5:1]. Samples were prepared by spin coating a given polymer mixture with 960 rpm for 5 min on microscopic glass slides. The thickness of these samples measured using VSI (vertical scanning interferometer, Bruker Contour Gt-X equipped with the Vision 64 software) was 30 µm. Oxygen plasma treatment of the PDMS samples was performed at 100 W for 10 s using a 4TEC plasma etcher (4-TEC Vakuum-Anlagenbau GmbH, Vierkirchen, Germany) and the resulting samples were stored at 30 °C. The motility experiments on the plasma-treated samples were carried out once the contact angle reached about 40°.

#### 2.1.4. SU-8

Microscopic glass slides were cleaned with acetone and IPA and subsequently air dried. After dehydration bake for 10 min at 200 °C the glass slides were treated with oxygen plasma for 5 min at 100 W. SU-8 3025 photoresist was spin-coated onto the slides using the Primus STT 15 Spinner. The spin coating parameters were 4000 rpm for 65 s to obtain a height of 15 µm. The spin coated substrates after soft bake for 14 min were flood exposed to 400 mJ/cm<sup>2</sup> of UV light using the mask-aligner (EVG@620 EV Group). Post exposure bake involved 1 min at 65 °C followed by 2 min at 95 °C and 1 min at 65 °C. Samples were developed in PGMEA (propylene glycol methyl ether acetate) for 20 min.

### 2.2. Bacterial strains and culture conditions

*Synechocystis* sp. PCC 6803 wild type from the Pasteur Culture Collection, originally acquired from the lab of S. Shestakov (Moscow, Russia) in 1993, was used in this study. Cells were spotted on motility plates prepared with 0.3% (w/v) agarose in BG11 medium [33] supplemented with 0.2% glucose, 0.3% sodium thiosulphate and 10 mM tris(hydroxymethyl)methyl-2-aminoethansulfonic acid (TES) (pH 8.0). The motility plate in an opaque box with a one-sided opening was placed in an incubator (Thermoshaker, Gerhardt, Germany) at 30 °C for at least 120 h. The plate was illuminated from the open side using three 525 nm LEDs (RGB LEDs, World Trading Net GmbH, Germany) with intensities in

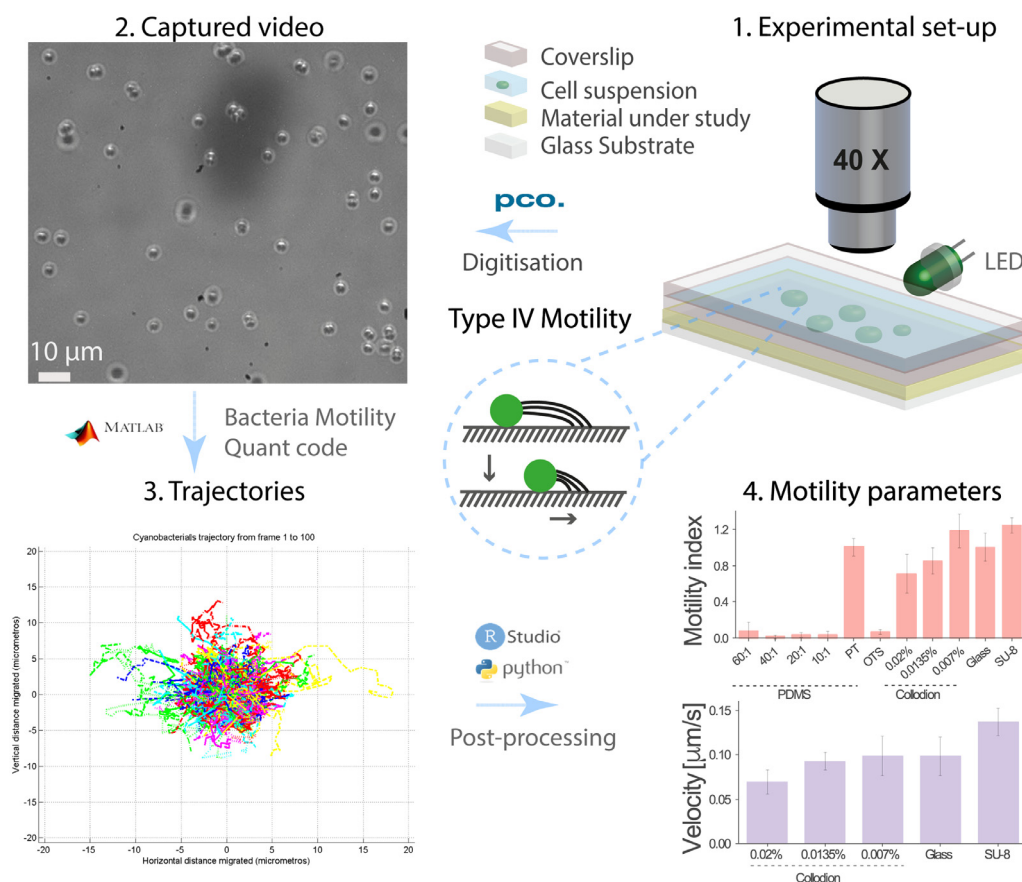


**Fig. 1.** Experimental set-up for phototaxis studies of *Synechocystis* cells and the subsequent image processing steps leading to relative motility measures. The motility index is defined as the ratio of the percentage of motile cells on the substrate under study to that on glass.

the range of 13.5 and 0.5  $\mu\text{mol photons m}^{-2} \text{s}^{-1}$ . After the incubation period, the bacteria showed positive phototaxis by forming finger-like projections [27]. For motility experiments, motile cells from the front of the fingers were re-suspended in fresh BG11. A 40  $\mu\text{l}$  drop of the suspension was dispensed on the substrate, and a coverslip (15  $\times$  15  $\text{mm}^2$ , Roth) was placed on top of it. After 5 min, the sides of the coverslip were sealed with nail polish to prevent evaporation. The sample was kept in the dark and was undisturbed for an additional 15 min before measurements. The mean value and standard deviation of the number of bacteria within the imaging field of view (2048 pixel  $\times$  2048 pixel) on each substrate are reported in Table A.1. The range is around 80–270 cells for the different substrates used in the study.

### 2.3. Phototaxis assay and motility quantification

The bacterial movement was imaged with a 40 $\times$  lens (40 $\times$ /.75NA, Nikon) mounted to a microscope (Ergolux200, LEICA). Videos were recorded with 1000 ms exposure for 5 min at 0.33 fps using a camera (Panda 4.2, PCO AG) fitted to the microscope shielded from ambient light using dark curtains. Before the measurements, cells were illuminated (525 nm, 11.1  $\mu\text{mol photons m}^{-2} \text{s}^{-1}$ ) at least 5 min from a single direction. The substrate was mounted on the microscope using a custom made holder fitted with 2 RGB LEDs (470/525/625 nm, World Trading Net GmbH) positioned on either side of the substrate to switch the light direction. The recorded bacterial movement was tracked using the BacterialMobilityQuant [3]. The resulting tracks obtained from the BacterialMobilityQuant were filtered using a customised script written in R (R CoreTeam, 2013) [34]. The filtering operation re-

moved cells that did not appear within 25 consecutive frames, cells faster than 0.4  $\mu\text{m s}^{-1}$  and cells showing displacement above 8  $\mu\text{m}$  between two frames. This protocol for processing the cell tracking to remove cells that show motion artifacts is taken from Schuergers et al. [3]. The fraction of motile cells from the filtered population was calculated with custom written Python code (Python Version 3.7.6 [35]). Bacteria were considered motile, if their velocity was above 0.05  $\mu\text{m s}^{-1}$ . Supplementary videos of phototaxis assay on SU-8, 10:1 PDMS (3 replicates) and Plasma PDMS have 50 times faster frame rate.

### 2.4. Surface characterization techniques

#### 2.4.1. Contact angle measurements

The contact angles of all the substrates discussed above were measured using three probe liquids, namely water, diiodomethane supplied by Thermo Fisher Scientific Chemicals, Inc. and glycerol (glycerin Rotipuran®  $\geq 99.5\%$ , Roth). A CS8620Ci, Teli camera equipped with a lens (Zoom 70XL microscope lens, Opto Sonderbedarf) was used to observe the suspended droplet. The contact angles were measured using the SCA20 (OCA) software. Three 3  $\mu\text{l}$  droplets were deposited on random locations per sample for each of the three probe liquids and the contact angles values were recorded. This was repeated three times for each kind of substrate used in the study. In order to plot the DLVO/XDLVO curves, the surface free energy components  $\gamma$  (see Section 2.4.2) values of the bacteria need to be known. To this end, contact angle measurements have been performed in a similar manner on a bacterial film grown on a microscope slide. Cells were diluted in BG11 and grown

on microscope slides for 120 h at 30 °C in the incubator. Then, they were left to dry at 30 °C for 1 h before the measurement.

#### 2.4.2. Surface energy calculations

From the measured contact angle values, surface energy was calculated using the Lifshitz–van der Waals (LW) acid-base approach [36] using the Cahn Radian DCA advantages software. Compared to other contact angle based surface energy techniques, the selected three-probe liquid approach not only yields the dispersive ( $\gamma^{LW}$ ) and polar ( $\gamma^{AB}$ ) components, but also splits the polar component in the electron acceptor ( $\gamma^+$ ) and electron donor components ( $\gamma^-$ ) of the surface free energy (Eq. (1)) [37].

$$(1 + \cos\theta)\gamma_l = 2\left(\sqrt{\gamma_s^{LW}\gamma_l^{LW}} + \sqrt{\gamma_s^+\gamma_l^-} + \sqrt{\gamma_s^-\gamma_l^+}\right) \quad (1)$$

Here,  $\theta$  is the measured contact angle value, and the indices  $s$  and  $l$  correspond to the surface and the liquid respectively. The values for  $\gamma_l^{LW}$ ,  $\gamma_l^-$  and  $\gamma_l^+$  of the probe liquids are generally known, as for instance reported in reference [38]. Then  $\gamma_l$  can be obtained from the summation of the dispersive ( $\gamma^{LW}$ ) and polar ( $\gamma^{AB} = \sqrt{\gamma^+\gamma^-}$ ) components of the liquid.

#### 2.4.3. Electrokinetic measurements and potentiometric acid/base titrations

Zeta-potentials of the tested flat surfaces were determined via streaming current measurements using the SurPass instrument (Anton Paar, Graz, Austria). Samples were cut to 10 mm × 20 mm rectangles. Two identical samples were glued on the stamps of the adjustable gap cell. Subsequently, the channel width was adjusted as close as possible to 100  $\mu$ m. A flow check was done to make sure that the pressure-flow relation was linear and identical from both flow directions. A titration in 1 mM NaCl solution, adjusted to pH 10 using 1 M NaOH was carried out down to pH 3 using 100 mM HCl titrant solution. Streaming current was measured with those samples. Each pH value involved 6 measurements (3 from each flow direction). The equilibration time prior to measurement was 900 s and during this time the channel was rinsed with the respective solution at a pressure of 100 mbar. In a second series of experiments, the objective was to determine the zeta-potential for the substrates in the relevant BG11 solution. This solution is complex and contains metal ions and molecules that will cause differences compared to 1 mM NaCl at the same pH whilst potentially contaminating the SurPass set-up. Consequently, the set-up was modified to avoid such contamination. More specifically, a two-step procedure was followed:

1. In the SurPass the gap cell was prepared as described above. A flow check was carried out and four measurements (with 6 runs each) at constant pH in 1 mM NaCl were carried out.
2. In a second set-up the gap cell was connected outside the SurPass instrument to the electrodes and an external pump (Legato 200) was used to generate pressure ramps from plastic syringes containing the target solution. The SurPass software was used to record the data in rinsing mode (i.e., pressure, current, voltage, and cell resistance, as well as pH and conductivity). This was first done using the same 1 mM NaCl solution used in step 1 to verify that the two set-ups gave identical results. Subsequently, the measurements were repeated in BG11 solution.

The electrokinetic behaviour of both the bacteria and the SiO<sub>2</sub> nanoparticle surrogates (since bacteria could not be glued to the tip) were analysed in suspensions using the Brookhaven nano apparatus. Measurements were carried out both using NaCl solution (1 mM) and BG11. The zeta-potentials were obtained using the Smoluchovsky equation. Additionally, potentiometric acid-base titrations of the bacteria were carried out again both in 1 mM NaCl

and BG11. A known volume of cell suspension was added to a solution of known volume to yield the desired electrolyte composition. Subsequently, the suspension was titrated by HCl solution of known concentration. To obtain the proton related surface charge, titration results for the same system without the cells were subtracted. In 1 mM NaCl, no measurable proton related charge was detected on the bacteria. In BG11 titrations (corrected for blank BG11 solution), a negative charge was observable.

#### 2.4.4. Surface roughness and thickness

A VSI (Vertical Scanning Interferometer, Bruker Contour Gt-X equipped with a Vision 64 software) was used to evaluate the 3D topography of various substrates based on the captured fringe patterns arising from the optical path length difference between the beam from the sample and the reference beam. A 2.27 mm<sup>2</sup> area was analysed with the Vision 64 software to determine the average roughness  $R_a$ . Measurements were performed on three spots per sample, with three samples per substrate.

#### 2.4.5. Rigidity

Nanoindentation measurements were performed using a Nanoindenter G200 (Keysight Technologies, Santa Rose, US). PDMS samples (see Section 2.1.3) were cut in 25 × 25 mm<sup>2</sup> pieces and mounted onto the test cylinders of the instrument. For each base to curing agent ratio, the sample was tested on at least 5 different locations. Due to the machine limitations in detecting the surface of the sample, two flat diamond punches with diameter  $D$  of 50  $\mu$ m and 20  $\mu$ m were used as indentation heads. The softer samples, 60:1 PDMS and 40:1 PDMS were tested with the bigger flat punch, while the other samples were tested with a smaller flat punch. The indentation depth was kept smaller than 10% of the PDMS film thickness accounting for the film/substrate system [39]. From the resulting slope  $S$  of the unloading curve, the reduced modulus  $E_r = S/D$  was calculated. Then, the elastic modulus of the sample  $E_s$  was determined by the equation

$$\frac{1}{E_r} = \frac{(1 - \nu_i^2)}{E_i} + \frac{(1 - \nu_s^2)}{E_s} \quad (2)$$

where the indices  $i$  and  $s$  refer to the diamond head and the PDMS sample, respectively,  $E$  denotes the Young modulus and  $\nu$  the Poisson ratio. These values have been calculated and reported in reference [40].

#### 2.4.6. X-ray photoelectron spectroscopy

XPS measurements were performed using a K-Alpha+ XPS spectrometer (ThermoFisher Scientific, East Grinstead, UK). The Thermo Advantage software was used for data acquisition and processing. All films deposited on glass substrate were analyzed using the Al K $\alpha$  line of a microfocused, monochromated X-ray source (400  $\mu$ m spot size). K-Alpha+ charge compensation system was employed during analysis, using electrons of 8 eV energy, and low-energy argon ions to prevent any localized charge build-up. The spectra were fitted with one or more Voigt profiles (binding energy (BE) uncertainty:  $\pm 0.2$  eV) and Scofield sensitivity factors were applied for quantification [41]. All spectra were referenced to the C 1s peak (C-C,C-H) at 285.0 eV binding energy controlled by means of the well-known photoelectron peaks of metallic Cu, Ag, and Au, respectively.

#### 2.4.7. AFM force-distance curves

The substrates were cut to 10 mm squares and glued onto AFM wafers. Force-distance measurements were performed in a liquid drop of BG11 solution, previously filtered with 0.2  $\mu$ m Sartorius®-filters. Colloidal AFM SiO<sub>2</sub> probes (Novascan®) of 877 nm diameter and 0.131(30) N m<sup>-1</sup> spring constant, calibrated by thermal tuning, were used during the measurements. The measurement parameters were set at a scan rate of 0.99 Hz and a trigger threshold of

65–100 nN. All AFM force measurements were performed with a Cypher Asylum Research AFM (Oxford instruments) at 30 °C. Force-distance curves were calculated as a heuristic approach. The potential effect of indentation during the measurements and subsequent effects on the presented forces was not further investigated as it is not the scope of this work. Therefore, we show preliminary force-distance curves calculating the tip-to-sample distance (“D”) as the sum of the piezo position ( $Z_p$ ) and the cantilever deflection ( $Z_c$ ), defining the zero-point based on the linear slope in the compliance region. The AFM measurements were performed in at least two different points over each surface, collecting around 10 curves per point. This was done in two independent occasions, roughly giving 30–60 curves per substrate.

### 2.5. DLVO and XDLVO theories of colloidal stability

The interactions between the bacteria and the surface can be studied using DLVO and XDLVO theories which provide the dependency between interaction energy and separation distance. The DLVO theory takes into account the effects of the Lifshitz–van der Waals forces and of the electrostatic double layer between the surface and the bacterium. The extended theory, XDLVO, additionally includes acid-base interactions and hydrophobicity effects. The equations pertaining to the DLVO/XDLVO theory are listed in the Appendix A.3. A series of experimental parameters is required in order to express the dependency between interaction energy and distance. The electrostatic effects are evaluated based on experimentally obtained zeta-potentials (see Section 2.4.3). Lifshitz–van der Waals and acid-base components of the surface energy are obtained from the contact angle measurements. The potential energy versus separation distance curves provided by the DLVO and XDLVO theories are important in predicting the behaviour of particles, in this case bacteria. In general, these curves may exhibit three regions of interest, defined with increasing separation: the primary minimum, primary maximum, and the secondary minimum. The primary minimum indicates the position of direct coalescence of particles, i.e., irreversible adhesion onto the surface, while the primary maximum is the potential barrier that prevents aggregation. The secondary minimum indicates reversible adhesion to the surface.

### 2.6. Statistical analysis

The measurement data are presented as mean values with standard deviation (SD) indicated via error bars unless stated otherwise.

## 3. Results

The multidimensional master plot presented in Fig. 2 summarises the main results of the present work. It constitutes the basis for further discussion and will be referred to throughout the following sections. For all the substrates considered in the present work, Fig. 2 relates bacterial velocity versus motility index, calculated as described in Section 3.1. As presented extensively in the introductory section, numerous factors may concomitantly influence bacterial adhesion and motility. Fig. 2 indicates the hydrophobic/hydrophilic character of each substrate that has been considered experimentally, split into three different value ranges of water contact angle. Another factor that has proven to influence bacterial behaviour on different substrates is the chemical composition of the surface. Fig. 2 includes the information relevant for surface chemistry, and must be seen in conjunction with the XPS discussion in Section 3.6. A full record of all measurements, assumptions and their comparison with existing reports can be accessed in the supplementary information, Table A.2.

### 3.1. Motility

The percentage of motile cells for each of the substrates is calculated as described in Section 2.3. Glass is used as a reference substrate because all other coatings (PDMS, collodion, SU-8 and OTS) have been deposited on the base microscope glass slides. Thus, the percentage of motile cells on glass is used to normalise the motile population of cells on the other substrates (motility index) included in Fig. 2. In this way, the results of this work are easily comparable to future studies if the same normalisation approach is used. The reference motility value on glass was obtained on the same day of the experiment as the respective normalised substrates. Glass has an average motile bacteria population of 51.8(83)%. SU-8 and plasma treated PDMS perform best in terms of velocity, and together with the lowest collodion concentration (0.007%) and the glass substrate form the group of substrates that perform best in terms of fraction of motile cells. Higher collodion concentrations reduce the number of motile cells: the 0.02% and 0.0135% collodion coatings are situated below the threshold of the motile cells on the reference glass substrate, while further increasing the concentration results in completely immotile cells (data points not shown in Fig. 2). This reduction can be attributed to the increase in the percentage of nitrogen atoms and will be discussed in conjunction with the XPS results in Section 3.6. There is a significant reduction of the motile cell population in all tested non-treated PDMS substrates (20:1, 40:1, 60:1 not shown in the graph due to very low motility values) and OTS. The average velocity of the cells on each substrate can also be inferred from Fig. 2.

### 3.2. Contact angle and surface energy calculations

The water contact angle (WCA) values for the substrates analyzed in this work are clustering around approximately 75° for SU-8 and different collodion dilutions, and around 116° for the PDMS variants, which is in agreement with literature [42,43]. OTS also is in the hydrophobic range of WCA with a value of 106.7°, whereas the plasma treated PDMS becomes hydrophilic with a WCA of 45.5° after 48 h of treatment. Glass is the most hydrophilic substrate presented in Table A.2 and in the master plot (Fig. 2) with 29.2°. Several other substrates with WCA values around 5° have been also analyzed, such as oxygen plasmatreated glass and commercially purchased super-hydrophilic substrates from Aquaray GmbH (Karlsruhe, Germany). We noticed that, for these substrates with a very pronounced hydrophilic character, cyanobacteria are floating within the liquid film formed on top, without exhibiting any adhesion or motility.

*Synechocystis* cells display a strong polar, electron donor character, with a considerably higher  $\gamma^{AB}$  over  $\gamma^{LW}$  and higher  $\gamma^-$  over  $\gamma^+$  (Table A.2). The glass and plasma treated PDMS substrates also show a less pronounced polar character, with the  $\gamma^{AB}$  component only slightly less than  $\gamma^{LW}$  and a rather strong hydrophilic behaviour. All other substrates exhibit more dispersive energy interactions (van der Waals, Keesom and Debye forces), with  $\gamma^{LW}$  on average one order of magnitude higher than  $\gamma^{AB}$ , and therefore have a hydrophobic tendency, with the SU-8 and the three collodion dilutions (0.007%, 0.0135% and 0.02%) falling in what we defined as the “moderate” range WCA values (diamond symbols in Fig. 2), and OTS and non-treated PDMS formulations in the hydrophobic range of WCA. In fact, lower values of the  $\gamma^{LW}$  component mean a weak dispersive attraction between the substrate and the bacterium and this is the most significant contribution to the total energy for all substrates considered.

A particular case is constituted by the collodion 0.2% dilution which exhibits WCA and  $\gamma$ -parameter values very similar to all substrates showing good motility of the bacteria population (SU-8, glass and the other three collodion dilutions). However, collodion

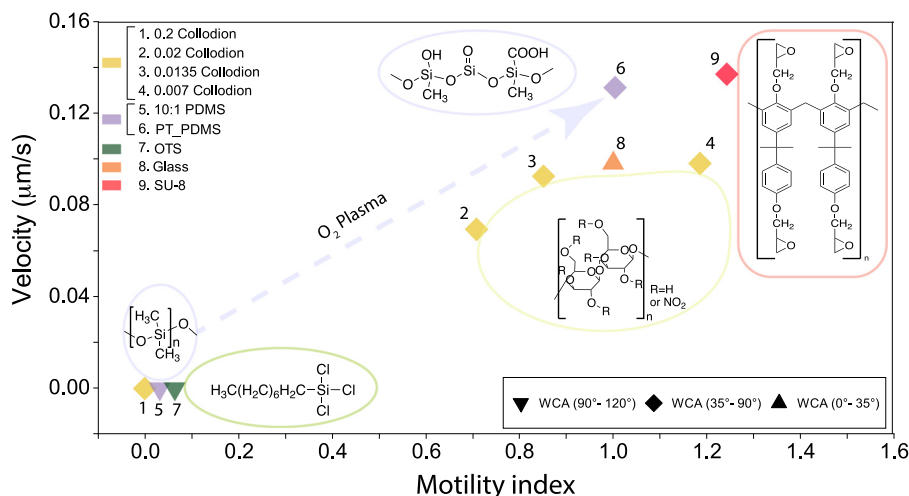


**Fig. 2.** The master plot is a scatter between the population of motile cells (motility index) versus the average velocity of the motile cells for the different substrates. The dimensionality of the plot is further extended by encoding the water contact angle (WCA) distributed in three ranges as the shape of the data point. Additionally, the colour of the markers signify substrates with a particular chemical nature and the chemical formulas are also indicated in the plot include in bubbles with the corresponding colour. The arrow indicates the shift in the motility index and cell velocity of the 10:1 PDMS sample after plasma treatment (PT-PDMS sample).

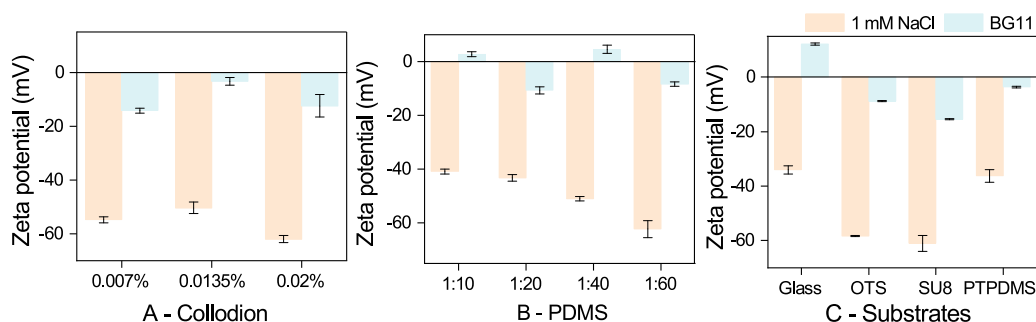


**Fig. 3.** Zeta-potential for A) collodion samples, B) PDMS samples C) glass, OTS, SU-8 and Plasma PDMS samples in NaCl solutions and BG11 medium in absence of cyanobacteria.

0.2% exhibit no significant motility of the bacteria population. Further XPS analysis in Section 3.6 is delineating the chemical composition differences of the collodion 0.2% substrate compared to the other collodion samples which show motility.

### 3.3. Electrokinetic measurements and potentiometric acid/base titrations

We performed zeta potential measurements to understand the electrostatic interactions between the bacteria and the surfaces. This approach has been performed in two steps, the first one determining the zeta-potential for suspensions with bacteria alone and the second one for surface behavior without cyanobacteria. Measurements have been performed in 1 mM NaCl solution, which is widely used as a standard for zeta-potential measurements, as well as in BG11 medium, which is the relevant medium in the present work and shown in Table A.2. Experimental results show that bacteria carry a net negative surface charge with zeta-potentials of  $-27$  mV in BG11 medium and  $-44$  mV in 1 mM NaCl at pH 8.0. The zeta potential of *Synechocystis* sp. PCC 6803 suspended in BG11 medium is stable for the relevant pH values (pH 7–9) as shown in Figure A.1. For the substrates studied in this paper, we have evaluated the zeta-potential in 1 mM NaCl and BG11 at pH 8.0 and the results are reported in Fig. 3 and tabulated in Table A.2 of the supplementary material. The measured zeta-potentials of OTS, SU-8 and glass substrates in NaCl are in good agreement with the literature [44–46]. The zeta-potential values for the collodion se-

ries in NaCl are around  $-60$  mV, and no measurements for comparison could be found in the existing literature. Fig. 3 shows a different behaviour of the surface charge when zeta-potential is measured in BG11 solution. While the measurements in BG11 exhibit rather large standard deviation and therefore no clear trend can be observed, they consistently suggest a less pronounced negative character of the analyzed substrates compared to the measurements in NaCl. Two aspects may explain this result. The ionic strength of the BG11 solution is about 20 mM (as estimated by a speciation calculation using the Geochemist's workbench coupled to the database covering the components present in the BG11 solution [47]) and an increase in the ionic strength will lower the magnitude of the zeta-potential in the absence of specific adsorption. Figure A.2 shows an example where the NaCl concentration has been set at 1, 10, and 20 mM in the PDMS 60:1 system. The independence of the isoelectric point as a function of the NaCl concentration indicates the absence of specific adsorption in the NaCl systems studied. The second aspect could be the composition of the BG11 solution. Compared to the monovalent electrolyte, the composition of BG11 is complex: the solution contains for example several multivalent cations at around  $\mu$ M concentration besides anionic components like EDTA (Ethylenediamine tetraacetic acid). The interaction of cations with the surface typically increases with pH. It can lead to charge inversion if the adsorption of these ions overcompensates the negative charge of the bare surface. According to the zeta-potential measurements, this occurs on glass, PDMS 10:1 and PDMS 40:1, while the plasma treated PDMS, PDMS 20:1,

and PDMS 60:1 have negative values. The SU-8, all collodion and OTS samples also retain a negative zeta-potential. The low negative zeta-potential values in BG11 compared to a non-specifically interacting solution of similar ionic strength (e.g. 20 mM NaCl in Figure A.2) might also be interpreted as a hint to specific adsorption. As the zeta-potential falls sharply in highly concentrated solutions, the effect of the electrostatic interaction energy between the bacterium and the surface would be low. Zeta-potential values determined here for bacteria and for each substrate in BG11 will be used in conjunction with the DLVO/XDLVO theory to obtain a quantitative understanding of the developed interaction forces, to be compared with the twitching motility results (see Section 4).

### 3.4. Surface roughness and thickness

An increase in surface roughness enlarges the available area for cell attachment. Higher roughness, when compared to the bacterium size, might create trap points on the surface or obstacles that hinder bacterial motility. The values for substrate thickness and the average roughness of the surfaces studied in this paper are given in Table A.3. The roughness of all layers considered is between 1 nm and 60 nm. As expected, glass and OTS form the smoothest surfaces with average roughness around 2 nm. Collodion samples had values in the range of 2 nm–10 nm. The value for SU-8 was about 19 nm for the spincoated thickness of 15  $\mu\text{m}$ . The 32  $\mu\text{m}$  thick PDMS samples had roughness values ranging from 16 nm to 26 nm. Additional treatment of PDMS with oxygen plasma promoted an increase in roughness to 42 nm, caused by the alterations introduced on the surface by plasma treatment.

### 3.5. Rigidity

In the next part, we report the Young's modulus of the different substrates used in this study. It has been previously demonstrated that the substrate rigidity influences the bacterial adhesion [48–50] therefore, we expect that rigidity will also have an influence on the bacterial motility. We study the impact of rigidity variation by tuning the PDMS composition. The systematic variation in PDMS rigidity is accomplished by different degrees of cross-linking of the PDMS elastomer base and curing agent. The reduction of the curing agent added to the polymer mix yields shorter polymer chains and hence lower stiffness. The stiffness of PDMS was quantified using nano-indentation measurements as mentioned in Section 2.4.5. The following Young's modulus values have been measured for base:curing agent weight ratios of 10:1, 20:1, 40:1, and 60:1, respectively: 1.970(200) MPa, 0.940(65) MPa, 0.660(13) MPa and 0.130(26) MPa. These results are similar to values reported in literature [51]. The rigidity of PDMS has been reported to increase by a factor of 4 after plasma treatment for 15 s [52]. The rigidity values from literature of glass and SU-8, used in this study are 76.4 GPa [53] and 5.9 GPa [54], respectively. The rigidity of the OTS substrates was assumed to be similar to the glass as the OTS is a nano meter thick mono-layer and this is confirmed by the shape of the force-distance curve by the AFM measurements discussed on Section 3.7. Although, no rigidity measurements were performed on the collodion substrates, the AFM measurements show that these substrates are softer compared to the glass surface.

### 3.6. X-ray photoelectron spectroscopy

All samples have been analysed by XPS analysis. Fig. 4 presents a selection of the relevant elemental spectra for the different substrates. All collodion samples, i.e. nitrocellulose, show a clear specific peak in C 1s at 287.4 eV attributed to -C-O-NO<sub>2</sub> present in collodion. Complementary N 1s at 408.0 eV and O 1s at 533.8 eV

support the presence of NO<sub>3</sub> groups. These peaks show an increase with collodion concentration. As expected the glass does not exhibit any nitrogen species but only some usual slight carbon contamination. The intensity of the silicon signal belonging to SiO<sub>2</sub> (Si 2p<sub>3/2</sub> at 103.0 eV) shows a decrease for the intermediate collodion concentrations and a sharp drop of 70% in comparison to the glass substrate for the highest collodion concentration (0.2%). This attenuation of the silicon signal is due to the formation of a collodion film on the glass (see Table A.3 for the thickness values). Similarly, for the glass modified with OTS, we can observe a decrease of the intensity of Si 2p<sub>3/2</sub> at 103.0 eV (SiO<sub>x</sub>). In addition, the contribution of C 1s at 285.0 eV increases dramatically from 6.6 atomic percent (at.%) for the clean glass up to 33.1 at.% in OTS, proving the attachment of the alkyl chain of OTS (Table A.4). At the same time, the underlying glass substrate is still detected since the layer is expected to be only a few nm thick. The SU-8 modified glass in Fig. 4 shows an intensive C 1s contribution at 286.8 eV of C-O additionally to the main C-C, C-H peak at 285.0 eV stemming from the aromatic rings and aliphatic carbons. The surface of PDMS was characterized by XPS before and after plasma treatment (see Fig. 4, bottom panels). Independently of the PDMS formulation, the pristine surface shows clearly only one main C 1s peak at 284.2 eV attributed to the methyl groups bound to silicon. The corresponding Si 2p doublet with Si 2p<sub>3/2</sub> at 101.6 eV (green area in Fig. 4) can be detected in a ratio 1.9:1 for CH<sub>3</sub>:Si close to the theoretical ratio of 2:1. Some SiO<sub>2</sub> is also detected in a weak concentration. After plasma treatment, two further components with low intensity appear at 286.1 eV and 288.9 eV, probably due to the oxidation of some methyl groups. Furthermore the C-Si content from C 1s decreases dramatically from 42.8 at.% to 12.8 at.% in the same manner as the corresponding Si-C species in Si 2p at 101.6 eV (Table A.4). Concomitantly, an increase of the contributions of SiO<sub>2</sub> species in Si 2p with Si 2p<sub>3/2</sub> at 103.0 eV (orange area in Fig. 4 Si 2p panel) can be observed, whereas the total oxygen content at the surface increases from 29.8 at.% up to 57.7 at.%. These observations support a replacement of -CH<sub>3</sub> groups by oxygen or hydroxide groups at the surface due to plasma treatment [55]. For the clean glass, the collodion and OTS modified glass substrates, also weak concentrations of Ca, Na, Sn, Zn and K can be detected as part of the glass (see Table A.4).

### 3.7. AFM force distance curves

Commercial AFM cantilevers with approximately 1  $\mu\text{m}$  diameter silica (SiO<sub>2</sub>) beads were used to investigate the forces between the silica tip and the different studied substrates in the presence of BG11 medium. The zeta-potentials of equivalent 1  $\mu\text{m}$  SiO<sub>2</sub> spheres (SSD4000, 1.05  $\mu\text{m}$  Silica (Dry), Bangs Laboratories Inc.) were -25 mV after suspending them in BG11. This is similar to the measured zeta-potential value of the bacterium in BG11 at pH 8 (see Section 3.3). Also, the shape and size of the bead are in a comparable range with the bacterium [3]. Thus, the silica beads from the cantilevers have been considered as substitutes to quantify the interaction force between the bacterium and the test substrates during AFM measurements. We report the approach force-distance curves in Fig. 5, showing quantitative information about potential interaction forces (e.g., van der Waals (VdW) forces, electrostatic forces). The potential effect of indentation during the measurements of certain soft surfaces (i.e., some PDMS and collodion sample types) is unknown and was not taken into account. The error bars include the variability of more than 30 replicated curves per condition, representing analytical and/or experimental variability for certain surfaces. The interaction between the complex components of BG11 solution and the surface functional groups (i.e. polymer chains, -NO<sub>3</sub> groups, aromatic rings and

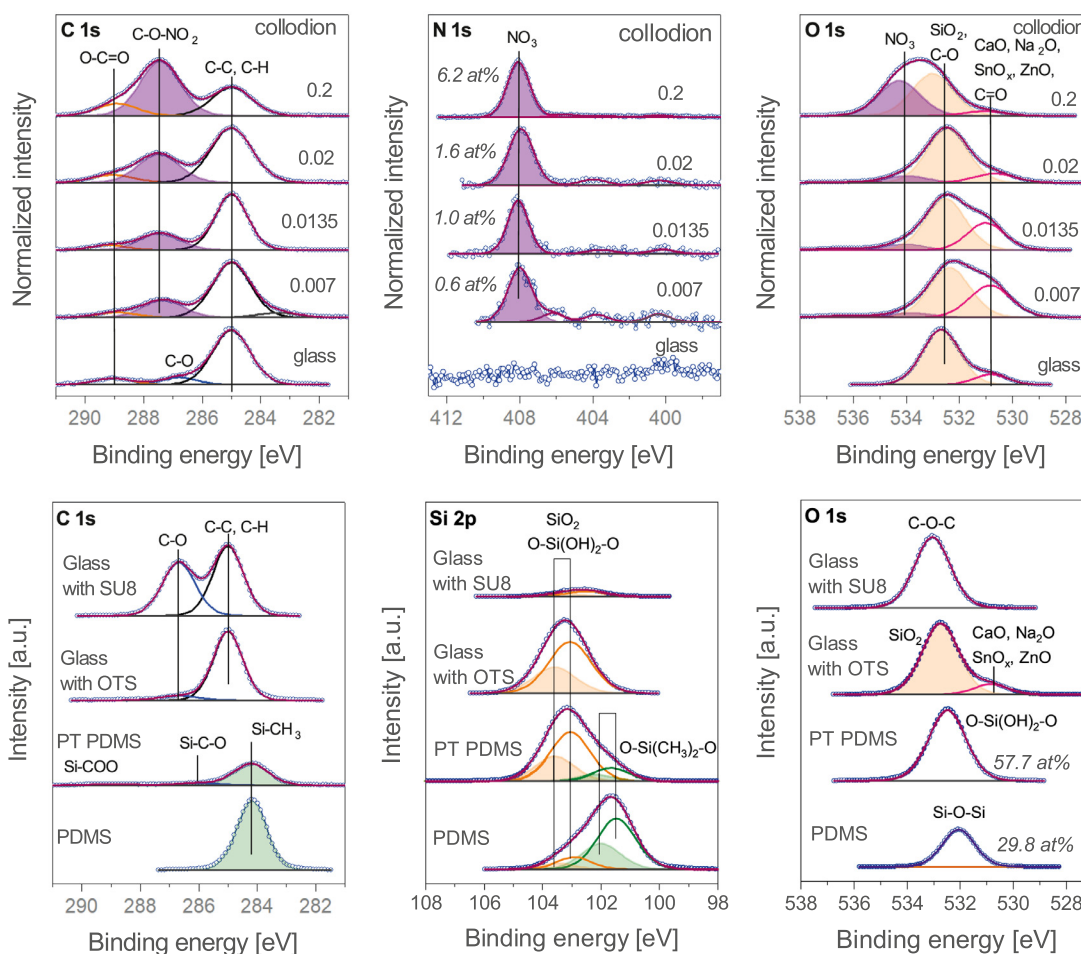


**Fig. 4.** C 1s, N 1s and O 1s XPS spectra of glass, collodion 0.007%, 0.0135%, 0.02% and 0.2% (top panel). C 1s, Si 2p and O 1s for PDMS, PT-PDMS, OTS and SU8 covered glasses (bottom panel). Most of intensities are normalized to the maximum.

**Table 1**

The adhesive force and their range of action measured during AFM retraction curves.

Sample	Estimated adhesive force (nN)	Range (nm)
PDMS series	$-181.0 \pm 37$	$1352 \pm 244$
PT-PDMS	-36.0	257
SU8	-25.5	183
Glass	-8.0	70
Collodion Series	$-6.8 \pm 4.6$	$66 \pm 33$
OTS	-0.4	5

aliphatic chains, described in Section 3.6) can explain the observed variability in the measurements.

Generally, VdW forces are only expected to appear in the lower range of separation (below 10 nm) [56]. The reference surface (glass) is the only surface showing weak VdW forces and probable electrostatic attraction (<10 nN) below 15 nm (i.e., in accordance with XDLVO calculations, see Discussion in Section 4). Only the OTS surface shows a fully repulsive regime, with no electrostatic repulsion apparent in the short range. The other surfaces (SU8, PT-PDMS, PDMS and collodion) rather show attractive VdW forces though probably not only related to electrostatic effects, in comparison with theoretical calculations (see Section 4). The adhesive forces quantified using the retraction force-distance curves are reported in Table 1 and the curves are shown in Figure A.3. The long range adhesive forces are practically absent for the OTS sample. The strongest adhesion is found for the native PDMS samples,

while the rest of the samples (PT-PDMS, SU8, glass, collodion series) have values in the range of  $-35$  nN to  $-5$  nN. The range of influence of these adhesive forces varies proportional to the measured force values (Table 1).

### 3.8. DLVO/XDLVO curves

DLVO/XDLVO theories are useful to understand the interactions between a bacterium and a surface. The DLVO theory takes into account the dispersive and electrostatic energies while the XDLVO additionally considers the acid-based energies between the bacterium and the surfaces in a liquid environment. The contributions of the energy components calculated from the contact angle measurements and the zeta-potential measurements in BG11 medium were inserted into the DLVO/XDLVO theories to yield the interaction energy (and hence the force) between the bacterium and the substrate as a function of distance. The DLVO/XDLVO force-distance curves are shown in Fig. 6, and the values and location of the energy (expressed as  $kT$ , where  $kT = 4.11 \times 10^{-21}$  J) and force minima are listed in Table A.5. The curves of the different substrates are grouped based on whether their water contact angles are less than (Fig. 6A and B) or greater than  $90^\circ$  (Fig. 6C and D). The XDLVO plot (Fig. 6A) of the hydrophilic surfaces show that there is no interaction between the bacterium and the surfaces for distances beyond 10 nm. However, at distances below 10 nm in all surfaces except glass, there is a sharp increase in the force thereby predicting a repulsive cell-substrate interaction. In the case of glass at distances below 10 nm, the bacterium experiences an attractive

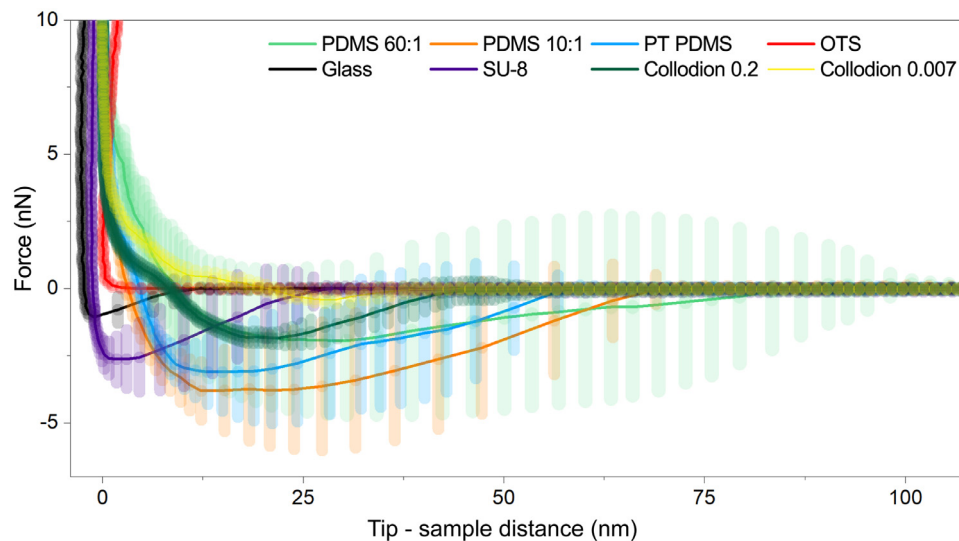


**Fig. 5.** AFM force-distance approach curves for all substrates against a  $\text{SiO}_2$  colloid probe in BG11 solution. The curves show short range (less than 10 nm) van der Waals forces and the electrostatic interactions averaged over 30 measurements per sample.

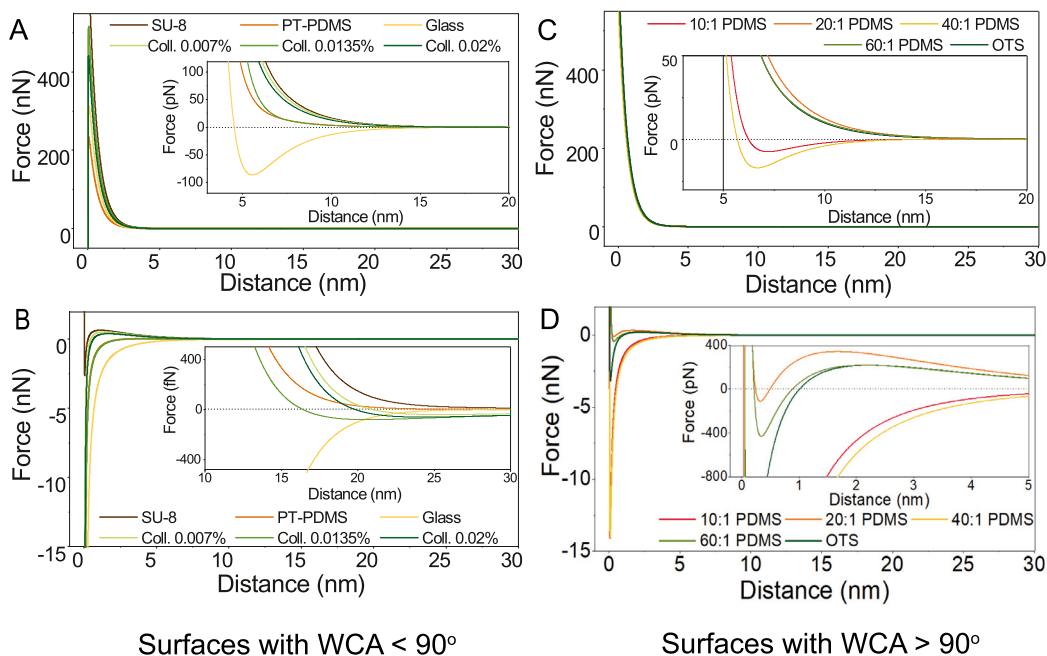


**Fig. 6.** The XDLVO and DLVO force plots for substrates with WCA less than  $90^\circ$  (A, B) and for substrates with WCA greater than  $90^\circ$  (C, D) respectively. The results from both XDLVO calculations (A,C) and DLVO calculations (B,D) are shown for all substrates, based on energy values derived from the contact angles and zeta-potential measurements in BG11. Respective insets are included to identify, if existing, the presence of secondary minima.

force slightly below 100 pN, but below 5 nm the force reverses to a repulsive one. Fig. 6C shows that the XDLVO curve of the hydrophobic 10:1 PDMS and 40:1 PDMS samples exhibit negligible attractive forces at distances less than 15 nm while being fully repulsive for the rest of the PDMS samples as well as OTS. The DLVO plots of the hydrophobic surfaces show a strong attractive force in the order of hundreds of pN to tens of nN at distances below 5 nm (Fig. 6D). The DLVO plots (Fig. 6B) of the hydrophilic surfaces are not relevant as they do not take into account the forces originating from the polar energy components, which cannot be neglected in the case of hydrophilic surfaces. Given the fact that only XDLVO calculations are comparable to the experimental AFM results (i.e. for the cases of glass and OTS), the DLVO theoretical calculations will not be discussed further in this work. Noteworthy, the possi-

bility of direct comparison between AFM curves and XDLVO could be somewhat limited for deformable samples. This means that differences between experimental AFM curves and theoretical XDLVO calculations may be both due to the complexity of the medium and the potential deformation of some of the softer surfaces, i.e., only applicable to some PDMS and collodion samples. In any case, these approximations don't invalidate the discussion of this work.

#### 4. Discussion

The motility experiments show that the motility index (fraction of motile bacteria with respect to the glass substrate) and the velocity of cyanobacteria are correlated, i.e. the data points corresponding to all substrates analysed are clustered in the up-

per right, and lower left quadrants of the graph presented in Fig. 2. Moreover, Fig. 2 is indicating that substrates with moderate hydrophilic WCA values are mostly favourable for cyanobacteria motility, more or less independent of the surface composition or functional groups (for further discussion see Section 4.2). All diamond symbols (substrates with WCA between 35° and 90°) in Fig. 2 except for 0.2% collodion and glass with a WCA of 30°, lie in the upper right quadrant of the graph, i.e., in the domain corresponding to highest velocity and highest motility index.

The motility behaviour of the bacteria depends on how the cell body and the pili individually interact with the surface. The comparison of the pilus-substrate and the cell body-substrate interaction forces help for a better understanding of how substrate properties affect the bacterial motility. The motility of the bacterium is an interplay between the cell body-substrate force and the retraction force exerted by the pili after attaching to the substrate. Even previous experiments from Nakane et al. showed that the bacteria on 0.2% collodion were immobilised, while the pili were able to extend and retract, thus gathering polystyrene beads closer to the cell body [32]. The results of this experiment suggest that the pili remain unaffected by the surface forces, and it is the force between the bacterial cell body and the surface that dictates the motility parameters. Thus, it is the net force interaction between the cell body with the substrate and the pilus retraction strength that dictates the motility.

#### 4.1. Interaction forces versus pilus strength

The motility behaviour of the bacteria on the different substrates was further interpreted in terms of the force-distance curves using the XDLVO theory. The XDLVO theory considers the interactions between the cell body and the substrate, while the interactions of the pili with the substrates are not considered. The magnitude of interaction forces between the cell body and the substrate, when compared with the forces that the pili of the bacterium can exert, may elucidate the behaviour of bacteria on the different substrates. Several papers have estimated the magnitude of the forces exerted by the pili. Using optical tweezers, the force that a single pilus can exert was quantified as 100 pN [57]. Similarly, force measurements on *N. gonorrhoeae* using a micropillar assay system report that multiple pili can generate forces up to 1 nN [58]. From the XDLVO plot for glass substrate in Fig. 6A at distances below 10 nm, the bacterium experiences an attractive force (slightly less than 100 pN) from the surface, which the force from the pili can overcome. This is in agreement with observed motility on glass (Fig. 2). The other hydrophilic substrates in Fig. 6A show that the bacterium experiences a repulsive force from these surfaces. However, this was not observed during AFM measurements (e.g. collodion and SU-8), where higher interaction forces were also recorded compared to the predicted forces from the XDLVO curves, despite the observed motility in Fig. 2. This implies that other forces beyond the polar, dispersive, and electrostatic are acting on the bacterium, but these are overcome by pili retraction forces. Although the XDLVO plots do not explain the bacterium-surface interactions in the case of the collodion and the SU-8 samples, the XPS studies can present an explanation for the observed motility patterns on these surfaces. In the collodion samples, the motility parameters (percentage of motile bacteria and their velocity) vary as a function of the concentration of the collodion. This variation is attributed to the change in the percentage of the NO<sub>3</sub> group confirmed by the XPS study (Fig. 4, N 1s panel). The high motility on the SU-8 substrate as seen in Supplementary Video S1 can be attributed to the prominent polar C-O sites present on the surface as seen in the C 1s panel of the SU-8 substrate.

The XDLVO curves of the hydrophobic PDMS substrates with varying base:curing agent ratios show no trend, due to the high uncertainty of the measured zeta-potential values in the BG11 medium. The XDLVO plots of these substrates show either negligible attraction (<20 pN) compared to the force exerted by the pili at distances below 10 nm or repulsive interaction. This interaction of the PDMS substrates with the bacterium, as predicted by the XDLVO plots, contradicts the experimental results for PDMS for both phototaxis and AFM approaches. During the phototaxis experiments, it was observed that bacteria appeared stuck onto the PDMS surfaces which have not been treated with oxygen plasma, i.e., in Fig. 2, these appear in the lower-left corner of the plot corresponding to low motility index and low velocity (Supplementary Videos S2, S3 and S4). The AFM approach force curve and the XDLVO force curve have a mismatch for the PDMS surfaces, due to the complexity of the medium and/or the potential deformation/indentation effects during the experimental measurements. The AFM approach curves confirm that the trapping of the bacteria at close separation distances is not only due to the VdW forces. We conjecture that a combination between these attractive forces (5 nN) and the stronger adhesive forces (180 nN) with a larger range of action explain the low motility of bacteria in PDMS. This is not the case for plasma-treated PDMS (as seen in Supplementary Video S5), where a simple change in the functional groups from -CH<sub>3</sub> to -OH significantly modifies the surface properties (i.e., hydrophilic surface with lower adhesion, showing higher mobility) compared to the original PDMS. That is, the XPS measurements suggest a preference of the cells for the hydroxyl groups (generated through the oxygen plasma process) over the methyl groups (existent prior to oxygen plasma). While there are no similar reports in the literature related to this behaviour, it is worth noting that it has been previously suggested [59] that plasma treatment of PDMS reduces adhesion of bacteria, which is in agreement with our observations. The work cited above [59] studies the adhesion of three different types of bacteria (*Escherichia coli* BL21, *Staphylococcus aureus* 6538, *Pseudomonas aeruginosa* ATCC 9027), and not their motility as in the present work. We consider that this result is relevant because the motility is influenced by adhesion.

For the case of OTS, both AFM and XDLVO calculations are in agreement (repulsive regime), however the experimental results show that there is no motility (Fig. 2). This also contrasts with the small recorded adhesive forces (Table 1), as it is counter-intuitive to not observe motility for surfaces where there are no signs of significant retention. However, incongruences between AFM and motility studies may be related to the hypothesis that the cells actually need some resistance/friction to grab/hold on to in order to move. This could explain why the highest mobility appears on SU-8 and PT-PDMS substrates (Table 1 indicating moderate adhesion forces around 30 nN) and the lowest in OTS (adhesion forces on OTS are insignificant - three orders of magnitude lower than SU-8 and PT-PDMS which makes OTS behave like a slippery surface for bacteria). Another possible explanation could be that physico-chemical characteristics of the substrate favour the transition from reversible to irreversible bacterial adhesion through bond-strengthening mechanisms [60]. Intermediate forces are not a challenge to the bacteria, they will be motile (e.g., higher mobility in SU-8 compared to collodion 0.02% is in accordance with the action range of registered forces, Table 1) and the range of action of the forces are relevant to cell motility.

#### 4.2. Key factors for designing adequate surfaces/substrates for phototaxis applications

The simultaneous visualisation of the different surface characterization measurements of the different substrates (SU-8, collodion 0.007%, plasma-treated PDMS, glass, OTS and 10:1 PDMS sub-

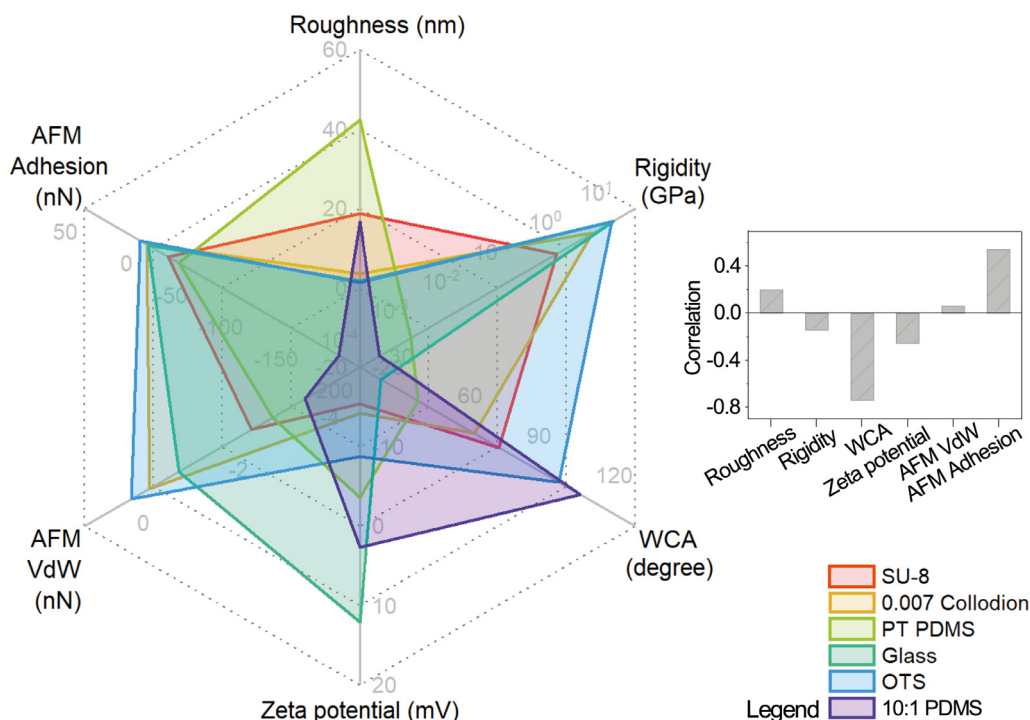


**Fig. 7.** The radar plot for the different substrates (SU-8, Collodion 0.007%, plasma-treated PDMS, glass, and OTS) listed in decreasing order of motility in the legend. Each of the axis represents one of the performed measurements. The rigidity is shown in a log scale, while the other axes are linear. The correlation of the normalised measurements with the motility index shows that the WCA and the AFM adhesion are the most relevant measurements in identifying substrates suitable for phototaxis.

strates listed in the decreasing order of motility) is shown in Fig. 7. The plot also shows the correlation values of the various characterization measurements with the quantified motility index. To enhance visualization, only the collodion 0.007% from the different collodion substrates is included in this plot as it exhibits the highest motility. Also, 10:1 PDMS is selected to represent PDMS substrates that did not support motility. Fig. 7 shows that the contributions of the measured VdW interactions has the least influence on the motility index. The influence of roughness and rigidity requires a more rigorous study that includes a wider range of roughness and Young's modulus. In the presented study, we did not observe significant influence of the roughness on the motility, and further investigation should be carried out independently. In the case of rigidity studies, even though PDMS has the lowest Young's modulus in the MPa range, motility favouring surfaces are generally those which are more rigid than PDMS, in the GPa range. From the inset bar plot, it can be noted that WCA and AFM adhesion measurements have the highest correlation with the motility index. This means that for future applications, measuring WCA and AFM adhesion are two strong indicators of bacterial motility, complemented by XPS measurements for surface chemistry investigation.

## 5. Conclusion

Our exhaustive surface characterisation study has identified that SU-8, a UV-sensitive epoxy routinely used in MEMS, which can be structured by means of standard UV lithography, has the maximum number of motile cells among all substrates analysed here-with. It is also important to note that SU-8 performs better than the lower 0.007% concentration of collodion, which has been previously studied in relation to phototaxis in cyanobacteria. Another remarkable result is the performance of the PDMS surfaces after oxygen plasma treatment, which is comparable in terms of motility with the normalised glass substrate, but even exceeds it in terms

of bacterium velocity. PDMS is another standard material extensively used for the fabrication of microfluidics, and more generally LOC systems, and oxygen plasma performed on PDMS is a standard process to change the surface chemistry and enhance hydrophilicity of the otherwise hydrophobic PDMS. A particularly useful conclusion for the cyanobacteria research community is that PDMS, a soft material widely used in LOC devices, and SU-8, a very popular MEMS material that can be easily structured by UV photolithography, are structural materials that are well-suited for cyanobacterial phototaxis studies, potentially offering better control and reproducibility compared to the traditional hydrogel-based assays.

## Declaration of Competing Interest

The authors declare that they have no known competing financial interests or personal relationships that could have appeared to influence the work reported in this paper.

## Acknowledgements

J.G.K. acknowledges primary support from the DFG under grant KO 1883/30-1, and partial support from ERC-SyG (HiSCORE, 951459), the framework of the German Excellence Initiative under grant EXC 2082 "3D Matter Made to Order", and the KIT-VirtMat initiative "Virtual Materials Design II". V.B. acknowledges partial support from HeiKA - HeiKA - Heidelberg Karlsruhe Strategic Partnership between Heidelberg University and KIT. We further acknowledge partial financial support of the Helmholtz Association through the programme "Materials Systems Engineering - MSE". ERM acknowledges support from the German Research Foundation (DFG) under grant number KO 1883/26-1. This work was supported by grants to A.W. under project no. WI 2014/8-1 and in frame of the SFB 1381 by the Deutsche Forschungsgemeinschaft (German Research Foundation) under project no. 403222702-SFB 1381 (A2). Authors thank Dr. Juan Li (IAM-WBM, KIT) for performing nano

indentation measurements and Mr. Richard Thelen (IMT, KIT) for the technical support for the VSI and contact angle measurements. All authors acknowledge the support of the Karlsruhe Institute of Technology (KIT), also through its publications fund, for providing the infrastructure to realise this work, and for a safe environment during the Covid-19 pandemic.

## Supplementary material

Supplementary material associated with this article can be found, in the online version, at doi:[10.1016/j.actbio.2022.10.035](https://doi.org/10.1016/j.actbio.2022.10.035).

## References

- [1] B.A. Whitton, *Ecology of Cyanobacteria II: Their Diversity in Space and Time*, Springer Science & Business Media, 2012.
- [2] A. Wilde, C.W. Mullineaux, Light-controlled motility in prokaryotes and the problem of directional light perception, *FEMS Microbiol. Rev.* 41 (6) (2017) 900–922, doi:[10.1093/femsre/fux045](https://doi.org/10.1093/femsre/fux045).
- [3] N. Schuergers, T. Lenn, R. Kampmann, M.V. Meissner, T. Esteves, M. Temerinac-Ott, J.G. Korvink, A.R. Lowe, C.W. Mullineaux, A. Wilde, Cyanobacteria use micro-optics to sense light direction, *Elife* 5 (2016) e12620, doi:[10.7554/eLife.12620](https://doi.org/10.7554/eLife.12620).
- [4] L. Craig, K.T. Forest, B. Maier, Type IV pili: dynamics, biophysics and functional consequences, *Nat. Rev. Microbiol.* 17 (7) (2019) 429–440, doi:[10.1038/s41579-019-0195-4](https://doi.org/10.1038/s41579-019-0195-4).
- [5] F.D. Conradi, C.W. Mullineaux, A. Wilde, The role of the cyanobacterial type IV pilus machinery in finding and maintaining a favourable environment, *Life* 10 (11) (2020) 252, doi:[10.3390/life10110252](https://doi.org/10.3390/life10110252).
- [6] Y. Yang, V. Lam, M. Adomako, R. Simkovsky, A. Jakob, N.C. Rockwell, S.E. Cohen, A. Taton, J. Wang, J.C. Lagarias, A. Wilde, D.R. Nobles, J.J. Brand, S.S. Golden, Phototaxis in a wild isolate of the cyanobacterium *Synechococcus elongatus*, *Proc. Natl. Acad. Sci.* 115 (52) (2018) E12378–E12387, doi:[10.1073/pnas.1812871115](https://doi.org/10.1073/pnas.1812871115).
- [7] N. Biais, D. Higashi, M. So, B. Ladoux, Techniques to measure pilus retraction forces, in: *Neisseria meningitidis: Advanced Methods and Protocols*, Humana Press, Totowa, NJ, 2012, pp. 197–216, doi:[10.1007/978-1-61779-346-2\\_13](https://doi.org/10.1007/978-1-61779-346-2_13).
- [8] A. Manz, N. Graber, H.Á. Widmer, Miniaturized total chemical analysis systems: a novel concept for chemical sensing, *Sens. Actuators, B* 1 (1) (1990) 244–248, doi:[10.1016/0925-4005\(90\)80209-1](https://doi.org/10.1016/0925-4005(90)80209-1).
- [9] E.T. Lagally, C.A. Emrich, R.A. Mathies, Fully integrated PCR-capillary electrophoresis microsystem for DNA analysis, *Lab Chip* 1 (2) (2001) 102–107, doi:[10.1039/b109031n](https://doi.org/10.1039/b109031n).
- [10] J. Park, V. Sunkara, T.-H. Kim, H. Hwang, Y.-K. Cho, Lab-on-a-disc for fully integrated multiplex immunoassays, *Anal. Chem.* 84 (5) (2012) 2133–2140, doi:[10.1021/ac203163u](https://doi.org/10.1021/ac203163u). PMID: 22277086
- [11] Z. Zhu, J.J. Lu, S. Liu, Protein separation by capillary gel electrophoresis: a review, *Anal. Chim. Acta* 709 (2012) 21–31, doi:[10.1016/j.aca.2011.10.022](https://doi.org/10.1016/j.aca.2011.10.022).
- [12] S. Lindström, H. Andersson-Svahn, Overview of single-cell analyses: microdevices and applications, *Lab Chip* 10 (2010) 3363–3372, doi:[10.1039/C0LC00150C](https://doi.org/10.1039/C0LC00150C).
- [13] M. Focke, F. Stumpf, B. Faltin, P. Reith, D. Bamarni, S. Wadle, C. Müller, H. Reinicke, J. Schrenzel, P. Francois, D. Mark, G. Roth, R. Zengerle, F. von Stetten, Microstructuring of polymer films for sensitive genotyping by real-time PCR on a centrifugal microfluidic platform, *Lab Chip* 10 (2010) 2519–2526, doi:[10.1039/C004954A](https://doi.org/10.1039/C004954A).
- [14] T.M. Norman, N.D. Lord, J. Paulsson, R. Losick, Memory and modularity in cell-fate decision making, *Nature* 503 (7477) (2013) 481–486, doi:[10.1038/nature12804](https://doi.org/10.1038/nature12804).
- [15] J. Männik, R. Driessen, P. Galajda, J.E. Keymer, C. Dekker, Bacterial growth and motility in sub-micron constrictions, *Proc. Natl. Acad. Sci.* 106 (35) (2009) 14861–14866, doi:[10.1073/pnas.0907542106](https://doi.org/10.1073/pnas.0907542106).
- [16] J.E. Keymer, P. Galajda, C. Muldoon, S. Park, R.H. Austin, Bacterial metapopulations in nanofabricated landscapes, *Proc. Natl. Acad. Sci.* 103 (46) (2006) 17290–17295, doi:[10.1073/pnas.0607971103](https://doi.org/10.1073/pnas.0607971103).
- [17] K.B. Gregory, D.R. Bond, D.R. Lovley, Graphite electrodes as electron donors for anaerobic respiration, *Environ. Microbiol.* 6 (2004) 596–604, doi:[10.1111/j.1462-2920.2004.00593.x](https://doi.org/10.1111/j.1462-2920.2004.00593.x).
- [18] D.R. Lovley, *Electromicrobiology*, *Annu. Rev. Microbiol.* 66 (1) (2012) 391–409, doi:[10.1146/annurev-micro-092611-150104](https://doi.org/10.1146/annurev-micro-092611-150104). PMID: 22746334
- [19] E.J. Stewart, Growing unculturable bacteria, *J. Bacteriol.* 194 (16) (2012) 4151–4160, doi:[10.1128/JB.00345-12](https://doi.org/10.1128/JB.00345-12).
- [20] J.Y.H. Kim, H.S. Kwak, Y.J. Sung, H.I. Choi, M.E. Hong, H.S. Lim, J.-H. Lee, S.Y. Lee, S.J. Sim, Microfluidic high-throughput selection of microalgal strains with superior photosynthetic productivity using competitive phototaxis, *Sci. Rep.* 6 (1) (2016) 21155, doi:[10.1038/srep21155](https://doi.org/10.1038/srep21155).
- [21] Y. Hanada, K. Sugioka, I. Shihira-Ishikawa, H. Kawano, A. Miyawaki, K. Midorikawa, 3D microfluidic chips with integrated functional microelements fabricated by a femtosecond laser for studying the gliding mechanism of cyanobacteria, *Lab Chip* 11 (2011) 2109–2115, doi:[10.1039/C1LC20101H](https://doi.org/10.1039/C1LC20101H).
- [22] Y.-T. Yang, C.Y. Wang, Review of microfluidic photobioreactor technology for metabolic engineering and synthetic biology of cyanobacteria and microalgae, *Micromachines* 7 (2016), doi:[10.3390/mi7100185](https://doi.org/10.3390/mi7100185).
- [23] F.B. Yu, L. Willis, R.M.W. Chau, A. Zambon, M. Horowitz, D. Bhaya, K.C. Huang, S.R. Quake, Long-term microfluidic tracking of coccoid cyanobacterial cells reveals robust control of division timing, *BMC Biol.* 15 (1) (2017) 11, doi:[10.1186/s12915-016-0344-4](https://doi.org/10.1186/s12915-016-0344-4).
- [24] L. De La Fuente, E. Montanes, Y. Meng, Y. Li, T.J. Burr, H.C. Hoch, M. Wu, Assessing adhesion forces of type I and type IV pili of *Xylella fastidiosa* bacteria by use of a microfluidic flow chamber, *Appl. Environ. Microbiol.* 73 (2007) 2690–2696, doi:[10.1128/AEM.02649-06](https://doi.org/10.1128/AEM.02649-06).
- [25] L.F. Cruz, J.K. Parker, P.A. Cobine, L. De La Fuente, Calcium-enhanced twitching motility in *Xylella fastidiosa* is linked to a single PilY1 homolog, *Appl. Environ. Microbiol.* 80 (23) (2014) 7176–7185.
- [26] A. Wilde, B. Fiedler, T. Börner, The cyanobacterial phytochrome Cph2 inhibits phototaxis towards blue light, *Mol. Microbiol.* 44 (2002) 981–988, doi:[10.1046/j.1365-2958.2002.02923.x](https://doi.org/10.1046/j.1365-2958.2002.02923.x).
- [27] M. Burriesci, D. Bhaya, Tracking phototactic responses and modeling motility of *Synechocystis* sp. strain PCC6803, *J. Photochem. Photobiol. B* 91 (2008) 77–86, doi:[10.1016/j.jphotobiol.2008.01.012](https://doi.org/10.1016/j.jphotobiol.2008.01.012).
- [28] R.M.W. Chau, D. Bhaya, K.C. Huang, G. Suel, E.G. Ruby, Emergent phototactic responses of cyanobacteria under complex light regimes, *mBio* 8 (2) (2017) e02330–16, doi:[10.1128/mBio.02330-16](https://doi.org/10.1128/mBio.02330-16).
- [29] L. Talá, A. Fineberg, P. Kukura, A. Persat, *Pseudomonas aeruginosa* orchestrates twitching motility by sequential control of type IV pili movements, *Nat. Microbiol.* 4 (2019) 774–780, doi:[10.1038/s41564-019-0378-9](https://doi.org/10.1038/s41564-019-0378-9).
- [30] A.E. Mattingly, A.A. Weaver, A. Dimkovič, J.D. Shrout, Assessing travel conditions: environmental and host influences on bacterial surface motility, *J. Bacteriol.* 200 (2018) e00014–18, doi:[10.1128/JB.00014-18](https://doi.org/10.1128/JB.00014-18).
- [31] W.-O. Ng, A.R. Grossman, D. Bhaya, Multiple light inputs control phototaxis in *Synechocystis* sp. strain PCC6803, *J. Bacteriol.* 185 (5) (2003) 1599–1607, doi:[10.1128/JB.185.5.1599-1607.2003](https://doi.org/10.1128/JB.185.5.1599-1607.2003).
- [32] D. Nakane, T. Nishizaka, Asymmetric distribution of type IV pili triggered by directional light in unicellular cyanobacteria, *Proc. Natl. Acad. Sci. USA* 114 (2017) 6593–6598, doi:[10.1073/pnas.1702395114](https://doi.org/10.1073/pnas.1702395114).
- [33] R. Rippka, J. Deruelles, J.B. Waterbury, M. Herdman, R.Y. Stanier, Generic assignments, strain histories and properties of pure cultures of cyanobacteria, *Microbiology* 111 (1) (1979) 1–61, doi:[10.1099/00221287-111-1-1](https://doi.org/10.1099/00221287-111-1-1).
- [34] RStudio Team, RStudio: Integrated Development Environment for R, RStudio, PBC, Boston, MA, 2020. <http://www.rstudio.com/>.
- [35] G. Van Rossum, F.L. Drake, Python 3 Reference Manual, CreateSpace, Scotts Valley, CA, 2009.
- [36] E. Lifshitz, M. Hamermesh, The theory of molecular attractive forces between solids reprinted from Soviet Physics JETP 2, Part 1, 73, 1956, in: L. Pitaevski (Ed.), *Perspectives in Theoretical Physics*, Pergamon, Amsterdam, 1992, pp. 329–349, doi:[10.1016/B978-0-08-036364-6.50031-4](https://doi.org/10.1016/B978-0-08-036364-6.50031-4).
- [37] C. van Oss, Hydrophobicity of biosurfaces—Origin, quantitative determination and interaction energies, *Colloids Surf., B* 5 (3) (1995) 91–110, doi:[10.1016/0927-7765\(95\)01217-7](https://doi.org/10.1016/0927-7765(95)01217-7).
- [38] C. Van Oss, R. Good, M. Chaudhury, The role of van der Waals forces and hydrogen bonds in “hydrophobic interactions” between biopolymers and low energy surfaces, *J. Colloid Interface Sci.* 111 (2) (1986) 378–390, doi:[10.1016/0021-9797\(86\)90041-X](https://doi.org/10.1016/0021-9797(86)90041-X).
- [39] G. Bruinsma, H. Van der Mei, H. Busscher, Bacterial adhesion to surface hydrophilic and hydrophobic contact lenses, *Biomaterials* 22 (24) (2001) 3217–3224.
- [40] Z. Wang, A.A. Volinsky, N.D. Gallant, Nanoindentation study of polydimethylsiloxane elastic modulus using Berkovich and flat punch tips, *J. Appl. Polym. Sci.* 132 (5) (2015), doi:[10.1002/app.41384](https://doi.org/10.1002/app.41384).
- [41] J. Scofield, Hartree–Slater subshell photoionization cross-sections at 1254 and 1487 eV, *J. Electron. Spectrosc. Relat. Phenomena* 8 (2) (1976) 129–137, doi:[10.1016/0368-2048\(76\)80015-1](https://doi.org/10.1016/0368-2048(76)80015-1).
- [42] Z. Gao, D.B. Henthorn, C.-S. Kim, Enhanced wettability of SU-8 photoresist through a photografting procedure for bioanalytical device applications, *J. Micromech Microeng* 18 (2008) 450131–450137, doi:[10.1088/0960-1317/18/4/045013](https://doi.org/10.1088/0960-1317/18/4/045013).
- [43] Y.J. Chuah, Y.T. Koh, K. Lim, N.V. Menon, Y. Wu, Y. Kang, Simple surface engineering of polydimethylsiloxane with polydopamine for stabilized mesenchymal stem cell adhesion and multipotency, *Sci. Rep.* 5 (1) (2015) 18162, doi:[10.1038/srep18162](https://doi.org/10.1038/srep18162).
- [44] J. Lützenkirchen, C. Richter, Zeta-potential measurements of OTS-covered silica samples, *Adsorption* 19 (2) (2013) 217–224, doi:[10.1007/s10450-012-9443-x](https://doi.org/10.1007/s10450-012-9443-x).
- [45] T. Sikanen, S. Tuomikoski, R.A. Ketola, R. Kostianen, S. Franssila, T. Kotiaho, Characterization of SU-8 for electrokinetic microfluidic applications, *Lab Chip* 5 (2005) 888–896, doi:[10.1039/B503016A](https://doi.org/10.1039/B503016A).
- [46] A. Sze, D. Erickson, L. Ren, D. Li, Zeta-potential measurement using the Smoluchowski equation and the slope of the current-time relationship in electroosmotic flow, *J. Colloid Interface Sci.* 261 (2003) 402–410, doi:[10.1016/S0021-9797\(03\)00142-5](https://doi.org/10.1016/S0021-9797(03)00142-5).
- [47] R.Y. Stanier, R. Kunisawa, M. Mandel, G. Cohen-Bazire, Purification and properties of unicellular blue-green algae (order *Chroococcales*), *Bacteriol. Rev.* 35 (2) (1971) 171–205, doi:[10.1128/br.35.2.171-205.1971](https://doi.org/10.1128/br.35.2.171-205.1971).
- [48] F. Song, D. Ren, Stiffness of cross-linked poly(dimethylsiloxane) affects bacterial adhesion and antibiotic susceptibility of attached cells, *Langmuir* 30 (34) (2014) 10354–10362, doi:[10.1021/ja502029f](https://doi.org/10.1021/ja502029f).
- [49] F. Song, M.E. Brasch, H. Wang, J.H. Henderson, K. Sauer, D. Ren, How bacteria respond to material stiffness during attachment: a role of *Escherichia coli* flagellar motility, *ACS Appl. Mater. Interfaces* 9 (27) (2017) 22176–22184, doi:[10.1021/acsami.7b04757](https://doi.org/10.1021/acsami.7b04757).

- [50] N. Saha, C. Monge, V. Dulong, C. Picart, K. Glinel, Influence of polyelectrolyte film stiffness on bacterial growth, *Biomacromolecules* 14 (2) (2013) 520–528, doi:[10.1021/bm301774a](https://doi.org/10.1021/bm301774a).
- [51] Z. Wang, A.A. Volinsky, N.D. Gallant, Crosslinking effect on polydimethylsiloxane elastic modulus measured by custom-built compression instrument, *J. Appl. Polym. Sci.* 131 (22) (2014), doi:[10.1002/app.41050](https://doi.org/10.1002/app.41050).
- [52] S. Vlassov, S. Oras, M. Antsov, I. Sosnin, B. Polyakov, A. Shutka, M.Y. Krauchanka, L.M. Dorogin, Adhesion and mechanical properties of PDMS-based materials probed with AFM: a review, *Rev. Adv. Mater. Sci.* 56 (1) (2018) 62–78, doi:[10.1515/rams-2018-0038](https://doi.org/10.1515/rams-2018-0038).
- [53] T. Adachi, S. Sakka, Dependence of the elastic moduli of porous silica gel prepared by the sol-gel method on heat-treatment, *J. Mater. Sci.* 25 (11) (1990) 4732–4737, doi:[10.1007/BF01129933](https://doi.org/10.1007/BF01129933).
- [54] R. Feng, R.J. Farris, The characterization of thermal and elastic constants for an epoxy photoresist SU8 coating, *J. Mater. Sci.* 37 (22) (2002) 4793–4799, doi:[10.1023/A:1020862129948](https://doi.org/10.1023/A:1020862129948).
- [55] B. Ruben, M. Elisa, L. Leandro, M. Victor, G. Gloria, S. Marina, S. Mian K, R. Pandiyan, L. Nadhira, Oxygen plasma treatments of polydimethylsiloxane surfaces: effect of the atomic oxygen on capillary flow in the microchannels, *Micro Nano Lett.* 12 (10) (2017) 754–757, doi:[10.1049/mnl.2017.0230](https://doi.org/10.1049/mnl.2017.0230).
- [56] X.-J. Zhang, *Van der Waals Forces*, Springer US, Boston, MA, 2013, pp. 3945–3947.
- [57] B. Maier, L. Potter, M. So, H.S. Seifert, M.P. Sheetz, Single pilus motor forces exceed 100 pN, *Proc. Natl. Acad. Sci.* 99 (25) (2002) 16012–16017, doi:[10.1073/pnas.242523299](https://doi.org/10.1073/pnas.242523299).
- [58] N. Biais, B. Ladoux, D. Higashi, M. So, M. Sheetz, Cooperative retraction of bundled type IV pili enables nanonewton force generation, *PLoS Biol.* 6 (4) (2008) 1–7, doi:[10.1371/journal.pbio.0060087](https://doi.org/10.1371/journal.pbio.0060087).
- [59] N. Lu, W. Zhang, Y. Weng, X. Chen, Y. Cheng, P. Zhou, Fabrication of PDMS surfaces with micro patterns and the effect of pattern sizes on bacteria adhesion, *Food Control* 68 (2016) 344–351, doi:[10.1016/j.foodcont.2016.04.014](https://doi.org/10.1016/j.foodcont.2016.04.014).
- [60] V. Carniello, B.W. Peterson, H.C. van der Mei, H.J. Busscher, Physico-chemistry from initial bacterial adhesion to surface-programmed biofilm growth, *Adv. Colloid Interface Sci.* 261 (2018) 1–14, doi:[10.1016/j.cis.2018.10.005](https://doi.org/10.1016/j.cis.2018.10.005).